Cellulose (2020) 27:4975–4990
https://doi.org/10.1007/s10570-020-03120-x

ORIGINAL RESEARCH

Nanocelluloses from phormium (*Phormium tenax*) fibers

Luciana Di Giorgio · Pablo Rodrigo Salgado · Alain Dufresne · Adriana Noemí Mauri

Received: 10 December 2019 / Accepted: 22 March 2020 / Published online: 30 March 2020

Abstract This work aimed in preparing nanocelluloses from a unique source of cellulose, viz. phormium (*Phormiun tenax*) fibers, by different techniques; and evaluate their physicochemical and structural properties. It was possible to obtain cellulose nanofibrils with different sizes (diameter, length and aspect ratio), morphology, crystallinity and surface charge by mechanical disintegration of bleached and refined phormium fibers previously modified or not with enzymatic and oxidative treatments with endoglucanases and 2,2,6,6-tetramethylpiperidine-1-oxyl (TEMPO), respectively. But it was not possible to prepare nanocrystals by acid hydrolysis, even when trying to modify the reaction conditions, possibly due at least partially to the presence of residual hemicelluloses and lignin. Process efficiency seemed to depend variably on the initial state of phormium (*Phormiun tenax*) fibers and the presence of other components such as lignin and hemicelluloses. These nanofibers could be used for different purposes in different areas according to their physicochemical characteristics.

L. Di Giorgio · P. R. Salgado · A. N. Mauri (✉)
Centro de Investigación y Desarrollo en Criotecnología de Alimentos (CIDCA), CONICET-Universidad Nacional de La Plata-CIC, 47 and 116 S/N°, B1900JJ La Plata, Argentina
e-mail: anmauri@quimica.unlp.edu.ar

A. Dufresne
CNRS, LGP2, Grenoble INP, Univ. Grenoble Alpes, 38000 Grenoble, France

Graphic abstract

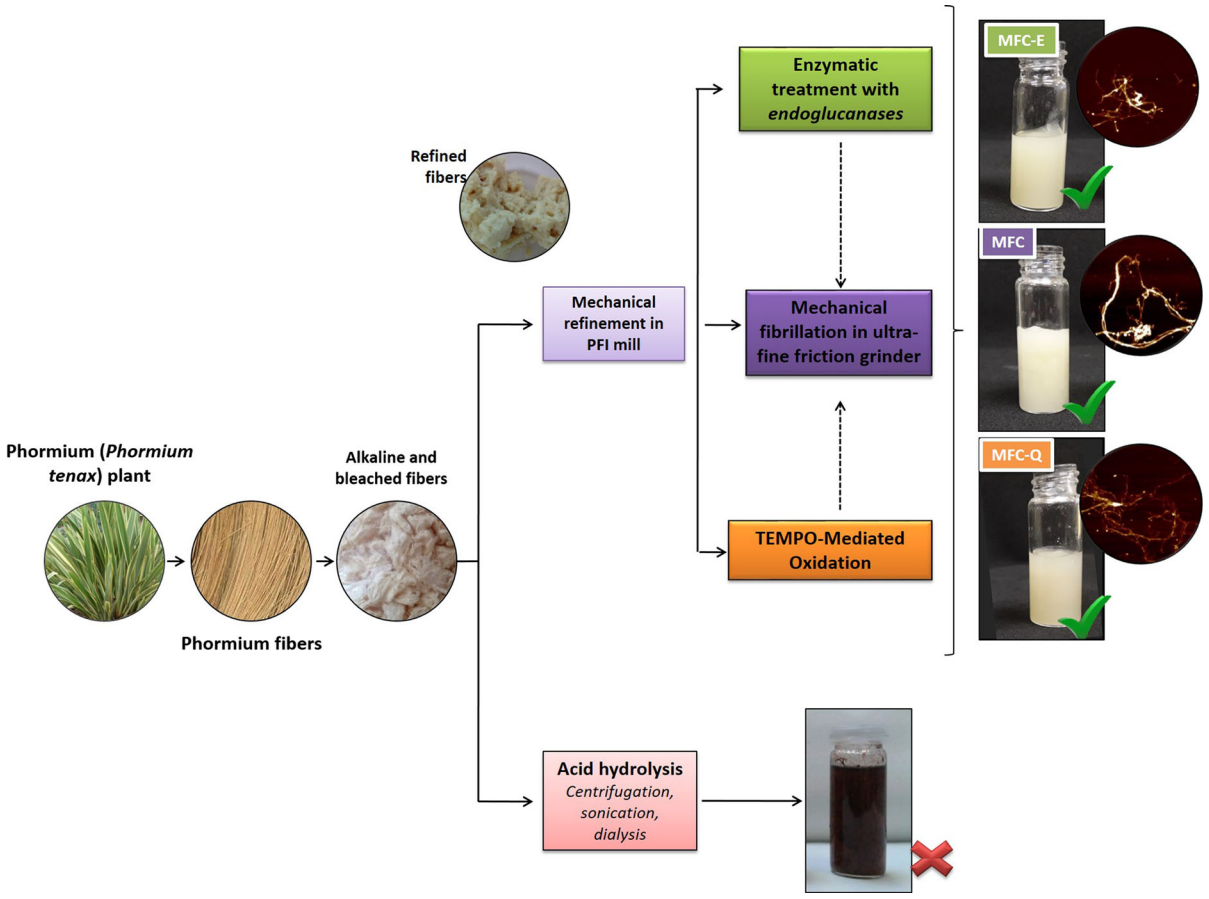

Keywords Nanocelluloses · Cellulose nanocrystals · Cellulose nanofibrils · Endoglucanases · TEMPO · Structural characteristics

Introduction

The interest for materials extracted from biological resources has grown enormously in recent years as a result of their high potential to manufacture high value products with low impact on the environment (Trache et al. 2017). Among natural biopolymers, cellulose is the most abundant, representing 50% of the biomass (Gómez et al. 2016). Although its exploitation has been known since the beginning of civilization, in the last decades it has attracted a lot of attention due to its versatility when processed at the nanoscale (Dufresne 2017). Cellulose is a linear high molecular weight homopolysaccharide formed by β-1,4-D-glucose units whose three free hydroxyl groups are capable of generating strong interactions through hydrogen bonds, which give cellulose a highly cohesive nature, and a microfibrillated organization. These microfibrils have usually nanoscale size and are composed of non-crystalline and crystalline zones, which are formed during the biosynthesis and packed by hemicelluloses, lignin and pectin substances (Thomas et al. 2018). In this way, the microfibrils are added to form the fibrils that constitute the majority component of the cell walls of plants, to which they give stiffness (Mishra et al. 2018).

Therefore, by understanding the structural organization of cellulose it is possible to obtain different types of nanocelluloses using different mechanisms and sources. Cellulose nanocrystals (CNCs) are nanostructures obtained by processing cellulose under controlled conditions (mainly by acid hydrolysis),

which lead to the release of individual crystals of high purity (Foster et al. 2018). Cellulose nanofibrils (CNFs), on the other hand, are prepared by mechanical shearing of cellulose fibers in order to separate the microfibrils in their constituent chains (Jawaid et al. 2017). By this way, long flexible cellulosic filaments are generated in the nanometric scale, with alternating non-crystalline and crystalline domains that cause a lower crystallinity and higher aspect ratio (L/d) than for CNC (Xie et al. 2018). Several pre-treatments of the fibers have been published in order to optimize CNFs production processes, trying to promote accessibility, increase the area of the internal surface, alter the crystallinity, break the hydrogen bonds and increase the reactivity of cellulose (Abdul Khalil et al. 2014; Jawaid et al. 2017). These pre-treatments reduce the energy consumption of the mechanical disintegration process and thus improve the degree of nanofibrillation (Nasir et al. 2017). These techniques include enzymatic treatments (with cellobiose, hydrolases and endoglucanases) (Tibolla et al. 2014; Beltramino et al. 2018); and chemical treatments such as oxidation with 2,2,6,6-tetramethylpipeline-1-oxyl (TEMPO) (Missoum et al. 2013; Rohaizu and Wanrosli 2017; Zhou et al. 2018), anionic modification with succinic anhydride (Sirviö and Visanko 2017), formic acid hydrolysis pretreatment (Du et al. 2016a), catalytic oxidation process based on the Fenton reaction (Li et al. 2018), etc. As a result of all these processes, nanocelluloses with varied characteristics in terms of shape and size, surface charge, crystallinity, mechanical resistance, etc., are obtained. These characteristics of the nanocellulosic materials represent a major opportunity for plant-based materials to improve their performance and functionality, and develop a new generation of products. This means that nanocellulose is a prime candidate for use as sustainable and recycling-based material in industries such as packaging, automotive components, biocomposites, reinforcement of composite materials, nanoporous filter media, higher strength papers for specific performance, facial masks for cosmetic applications, sensors, acoustic diaphragms, rheology modifiers, biomedicine and food ingredients (Jawaid et al. 2017; Kasiri and Fathi 2018; Niu et al. 2018).

There is a particular interest in obtaining these nanocelluloses from economic sources. Phormium (*Phormiun tenax*) is a perennial monocotyledonous herbaceous plant that grows mainly in well-drained soils and vicinity of swamps, but can grow almost anywhere and is widespread in gardens, such as the perennifolia decorative plant (Fig. 1a). Long fibers can be obtained from its leaves, that have been mainly used in the textile and paper industry (Fortunati et al. 2013). They have also been used extensively in composites formulation (De Rosa et al. 2010), and more recently in CNCs and CNFs preparation for their use in nanocomposites (Fortunati et al. 2013, 2014; Ortiz et al. 2018). However, nanofibers reported in these studies were prepared from fibers that were differently pre-treated (to separate lignin and hemicelluloses) and processed. So, the aim of the present work was to prepare nanocelluloses from phormium (*Phormiun tenax*) fibers by different techniques including hydrolysis and mechanical disintegration, with and without TEMPO or enzymatic pretreatments, using the same source of fibers, evaluate their physicochemical and structural properties, and analyze how the presence of residual lignin and hemicelluloses affect process efficiency.

Materials and methods

Materials

Phormium fibers (*Phormium tenax*) grown in Tigre (Buenos Aires, Argentina) and purchased from Silkum (Argentina) were used as raw material.

The enzymatic and oxidative treatments were carried out with endoglucanases (FiberCare® R 4760 UE, Novozyme, Denmark) and 2,2,6,6-tetramethylpiperidine-1-oxyl (TEMPO, Sigma-Aldrich), respectively.

The other reagents used were of analytical quality.

Alkali and bleaching pre-treatments of phormium fibers

Initially, *Phormium tenax* fibers were submitted to a washing pre-treatment to remove impurities and waxy substances covering the external surface of fiber cell walls. They were chopped to an approximate length of 5–10 mm and dispersed in 1 M NaOH (5% w/v) at 80 °C for 2 h using an overhead stirrer (OS20-Pro, DragonLab, China) at 500 rpm. The resulting suspension was filtered (270 mesh) and washed with cold water. This procedure was repeated twice. As lignin

Fig. 1 Phormium (*Phormium tenax*) plant (**a**), untreated phormium fibers used in this study (**b**), alkali treated and bleached fibers (**c**), and refined fibers (**d**)

hinders fiber separation, partial delignification (bleaching) was performed in order to facilitate further cellulose nanofiber preparation. Pre-treated fibers were dispersed (5% w/v) in 3% v/v H_2O_2 at 80 °C at 500 rpm (OS20-Pro, DragonLab, China) for 30 min, then cooled in an ice bath, filtered (270 mesh) and washed with cold water. This procedure was also repeated twice. Bleached fibers were dried at 80 °C for 15 h in an oven with air flow circulation (Yamato, DKN600, USA).

Phormium fiber composition

The chemical composition of initial and bleached phormium fibers was determined. A cellulose suspension in water was first prepared and dried in an oven at 60 °C until it reached a constant weight, and the organic solvent soluble compounds were extracted from the dried sample by Soxhlet technique using initially ethanol 96%, then ethyl acetate and finally hexane. These Phormium fibers (2 g) were firstly treated with 0.6% w/v of sodium chlorite with 63 mL of distilled water and were heated at 70–80 °C for 1 h. The pH of the solution was lowered to about 4 by means of acetic acid for the bleaching. This treatment was repeated two more times and then the fibers were dried in an oven at 60 °C. At the end of this preliminary chemical process, holocellulose (α-cellulose and hemicellulose) was obtained. The holocellulose was treated with 17.5% w/v NaOH solution and acetic acid 10% (ANSI/ASTM, 1977), filtered and washed with distilled water. The obtained cellulose was dried at 60 °C in an oven until constant weight. The moisture and ash values were determined gravimetrically, using the AOAC 935.29 and AOAC 923.03

methods (AOAC: Association of Official Analytical Chemists Inc., 1995).

Cellulose nanocrystals (CNCs) preparation by acid hydrolysis

Bleached phormium fibers were dispersed in a 5% w/v ratio of H_2SO_4 solutions of different concentrations (50, 55, 60, 65% w/w), and kept under continuous stirring at 350 rpm with a propeller stirrer up to 5, 10, 15, 30 and 45 min at 45 °C under hood.

Cellulose nanofibril (CNF) preparation by mechanical disintegration

Three batches of cellulose nanofibrils were prepared. Initially, the bleached cellulose fibers were subjected to a refining process in a Papirindustriens Forskningsinstitutt (PFI) mill to improve the fiber accessibility and the efficiency of the mechanical fibrillation process. Subsequently, one of the batches was subjected to an enzymatic treatment with endoglucanases, and another to an oxidizing chemical treatment. Finally, the three batches were subjected to the mechanical fibrillation process. Products obtained were labeled CNF, CNF-E and CNF-T, respectively.

PFI mill refining treatment

The bleached fibers were hydrated with distilled water (10% w/v) for 24 h and refined in a beater (NPFI-02, PFI, Metrotec, France) under a refining pressure of 3.33 N/mm and a speed of 9000 rpm, corresponding to a desired refining grade value of $\approx$ 70°SR (ISO 5267-1: 1999). Finally, the PFI mill was stopped and phormium fibers were manually separated.

Enzymatic treatment

A 2 L aqueous suspension of bleached and refined fibers (2% w/v) was placed in a three neck round bottom flask with balloon with 2 mL of endoglucanase-type enzyme solution and acetate buffer at pH = 5. The endoglucanase acts on the amorphous region of cellulose to hydrolyze the β-1,4-glycosidic bond, so the long cellulose chains are truncated into smaller molecular weight cellulose in the interior of cellulose. The enzymatic reaction was carried out at 50 °C for 120 min with continuous stirring at 350 rpm and thermally stopped at 80 °C for 10 min. The suspension was cooled and filtered in a Buchner funnel using a nylon sieve of 10 μm pore size and the retained solid was washed with distilled water until achieving a pH close to neutrality. Finally, the suspension was stored at 4 °C for 24 h before being mechanically fibrillated.

TEMPO-mediated oxidation of cellulose

A 1.5 L aqueous suspension of bleached and refined fibers (1% w/v) was placed in a three neck round bottom flask with balloon with 0.24 g of 2,2,6,6-tetramethylpiperidine-1-oxyl (TEMPO) and 1.5 g of NaBr and stirred for 10 min until the complete dissolution of the reactants was achieved. Subsequently, 5.58 g of NaClO were added and the pH was adjusted to 10 with 3 M NaOH. The reaction was kept under stirring at 350 rpm, for 2 h at 25 °C and stopped by lowering the pH of the suspension to 7 with 3 M HCl. The suspension was filtered in a Buchner funnel using a nylon sieve of 10 μm pore size and the retained solid was washed with distilled water until achieving a constant conductivity of 5 μS/cm. Finally, the suspension was stored at 4 °C for 24 h before being mechanically fibrillated.

Mechanical fibrillation with ultra-fine friction grinder

Suspensions of bleached and refined fibers and of those subjected to pretreatments were nanofibrillated. This process was carried out using an ultra-fine friction grinder (Masuko Sangyo Super Masscollider, MasukoSangyo Co, Japan). The suspension containing $\approx$ 1–2% refined fibers passed through the devise at a rotation of 2500 rpm. The total number of passes was 130 with a *gap* between 0 and − 1 during the process. Cellulose nanofibril suspension samples with drops of chloroform (as antimicrobial) were refrigerated at 4 °C until their characterization. Table 1 summarizes the nomenclature used for the different nanofibers.

Cellulose nanofiber characterization

Solid content

A specified amount of the suspension was collected and weighed before and after oven drying at 105 °C

Table 1 Codification of the different nanofibers prepared from phormium (*Phormium tenax*) fibers by different treatments

Nomenclature	Treatments					
	Alkali and bleaching treatment	Acid hydrolysis	PFI mill refining treatment	Enzymatic treatment with endoglucanases	TEMPO-mediated oxidation	Mechanical fibrillation
CNC	✔	✔				
CNF	✔		✔			✔
CNF-E	✔		✔	✔		✔
CNF-T	✔		✔		✔	✔

for 24 h. The solid content (%) was determined in duplicate for each sample, and calculated as the percentage of weight retained to the original weight.

Process yield

The process yield was determined by relating the solid content of the final dispersion with respect to the solid content of the initial dispersion or raw material. Determinations were done in duplicate.

Appearance and morphological analysis

The suspensions of nanofibers and some intermediate products of the processes were photographed with a digital camera to reveal their macroscopic aspect.

The morphology of the samples was observed by atomic force microscopy (AFM). One drop (20 μL) of the fiber dispersion was placed on a mica sample holder and dried under a nitrogen stream. The samples were analyzed with a NanoScope III device (Veeco Instruments, China), in tapping mode, using a silicon cantilever probe. The diameter and length of the nanofibers were calculated from the images using the Nanoscope 6.13 software. Determinations were done at least in duplicate.

Z-potential

Determinations were carried out in a nanoparticle analyzer (Nanopartica SZ-100 series, Horiba, Japan) at room temperature, diluting the samples with distilled water (1/1000). Ten replicates were made for each sample.

X-ray diffraction

The X-ray diffraction spectra of the nanofibers were obtained with a X'Pert Pro diffractometer (PANalytical, USA) equipped with a CuKα radiation source (λ = 0.154 nm). The voltage and current used were 40 kV and 40 mA, respectively. The diffraction data were obtained in the range 2θ = 5°–40° in a fixed time mode with a step interval of 0.10°, at a step speed of 1.2°/min.

The X-ray diffraction (XRD) spectra were used to calculate the crystallinity index (CrI) according to Eq. 1, using the intensity values corresponding to the diffraction of the crystalline structure and the amorphous fraction, according to the Segal equation as described by Park et al. (2010):

$$\mathrm{CrI} = \frac{(\mathrm{I}_{200} - \mathrm{I}_{\mathrm{am}})}{\mathrm{I}_{200}} \quad (1)$$

where I_{200} is the maximum intensity of the crystalline peak located at 2θ = 22°–23°, and I_{am} is the intensity of the valley located at 2θ between 18° and 19° (main zone).

The determinations were made in duplicate.

Attenuated total reflectance–Fourier transform infrared spectroscopy (ATR-FTIR)

Cellulose nanofiber samples were placed on the ATR diamond crystal (Smart iTX accessory, ThermoScientific, Waltham, MA, USA) and FTIR spectra were recorded in the region 4000–400 cm^{-1}, using a ThermoNicolet iS10 spectrometer (ThermoScientific, Waltham, MA, USA), performing 60 scans per test with a resolution of 4 cm^{-1} at room temperature. The obtained spectra were analyzed with Omnic Specta

software (Nicolet Instrument Co., Madison, WI, USA). Determinations were made at least in triplicate.

Statistical analysis

The results were expressed as average value ± standard deviation and analyzed by analysis of variance (ANOVA). The average values were evaluated by the Tukey test for comparison of pairs, with a level of significance $\alpha = 0.05$. For this, the Statgraphics Centurion program, version 16.1.18 (Statgraphics, USA) was used.

Results and discussion

Alkaline and bleaching initial pre-treatments

Table 2 shows the initial fibers composition. These fibers showed a high cellulose and hemicelluloses content ($\approx$ 46 and 38%, respectively) but also an important lignin content ($\approx$ 10%), similar to the values reported by Fortunati et al. (2013). In order to isolate cellulose, alkaline and bleaching pre-treatments were carried out. The alkaline treatment was performed to eliminate hemicelluloses and other soluble impurities that cover the external surface of the cell walls of the fibers (Zainuddin et al. 2013), and the bleaching treatment with H_2O_2 to remove residual materials, mainly lignin (Panaitescu et al. 2013). This latter pre-treatment was preferred to the one performed by Fortunati et al. (2013) using $NaClO_2$ for being less toxic and more environmentally friendly. Although the pre-treatments used in this work succeeded in reducing the initial hemicelluloses and lignin contents, which were $\cong$ 56 and 53, % respectively, the bleached fibers still contain almost 17 and 5% of these components (Table 2).

Figure 1 shows photographs of phormium plant, its untreated fibers used in this study, the alkaline and bleached forms of these fibers and their refined form.

Figure 1 shows how the appearance of the fibers changed during these initial treatments to obtain bleached cellulose. Initial fibers (Fig. 1b) showed their typical brown coloration and appearance, similar to that published by other authors (De Rosa et al. 2010). The alkaline and bleaching treatments contributed to their discoloration due to the partial elimination of hemicelluloses and lignin, and their agglomeration as a result of the washing and subsequent drying (at 80 °C) stages (Ortiz et al. 2018) (Fig. 1c, d).

Cellulose hydrolysis

Cellulose nanocrystals (CNCs) are mainly prepared by strong hydrolysis with H_2SO_4, which leads to the release of individual crystals of high purity (Abdul Khalil et al. 2014). During this process the acid diffuses into the fibers and splits the glycosidic bonds of the non-crystalline regions of cellulose while the crystalline zones remain intact (Börjesson and Westman 2015). This acidic treatment also induces the esterification of some of the hydroxyl groups with sulfate groups on the surface of the fibers and these charged residues, whose density increases with the severity of the treatment (acid concentration, time, temperature), are responsible for the stability of the resulting aqueous CNC suspensions (Dufresne 2017). In order to obtain CNCs from bleached phormium fibers, different hydrolysis conditions were studied in the range of those used in the literature for this purpose (Bondeson et al. 2006; Fortunati et al. 2013; Mishra et al. 2018). Figure 2 shows the appearance of the dispersions treated for different durations with different acid concentrations.

Table 2 Cellulose (%), hemicelluloses (%), lignin (%), moisture (%) and ash (%) content of initial phormium fibers, and alkali treated and bleached phormium fibers

	Cellulose (%)	Hemicelluloses (%)	Lignin (%)	Moisture (%)	Ash (%)
Initial Phormium fibers	46.17 ± 3.16^{a}	38.14 ± 1.52^{b}	10.36 ± 1.64^{b}	4.76 ± 0.71^{a}	0.58 ± 0.06^{a}
Bleached Phormium fibers	73.73 ± 0.29^{b}	16.94 ± 0.55^{a}	4.86 ± 0.12^{a}	4.69 ± 0.01^{a}	0.52 ± 0.08^{a}

Values with different letters in the same column are significantly different ($p < 0.05$) according to the Tukey's test

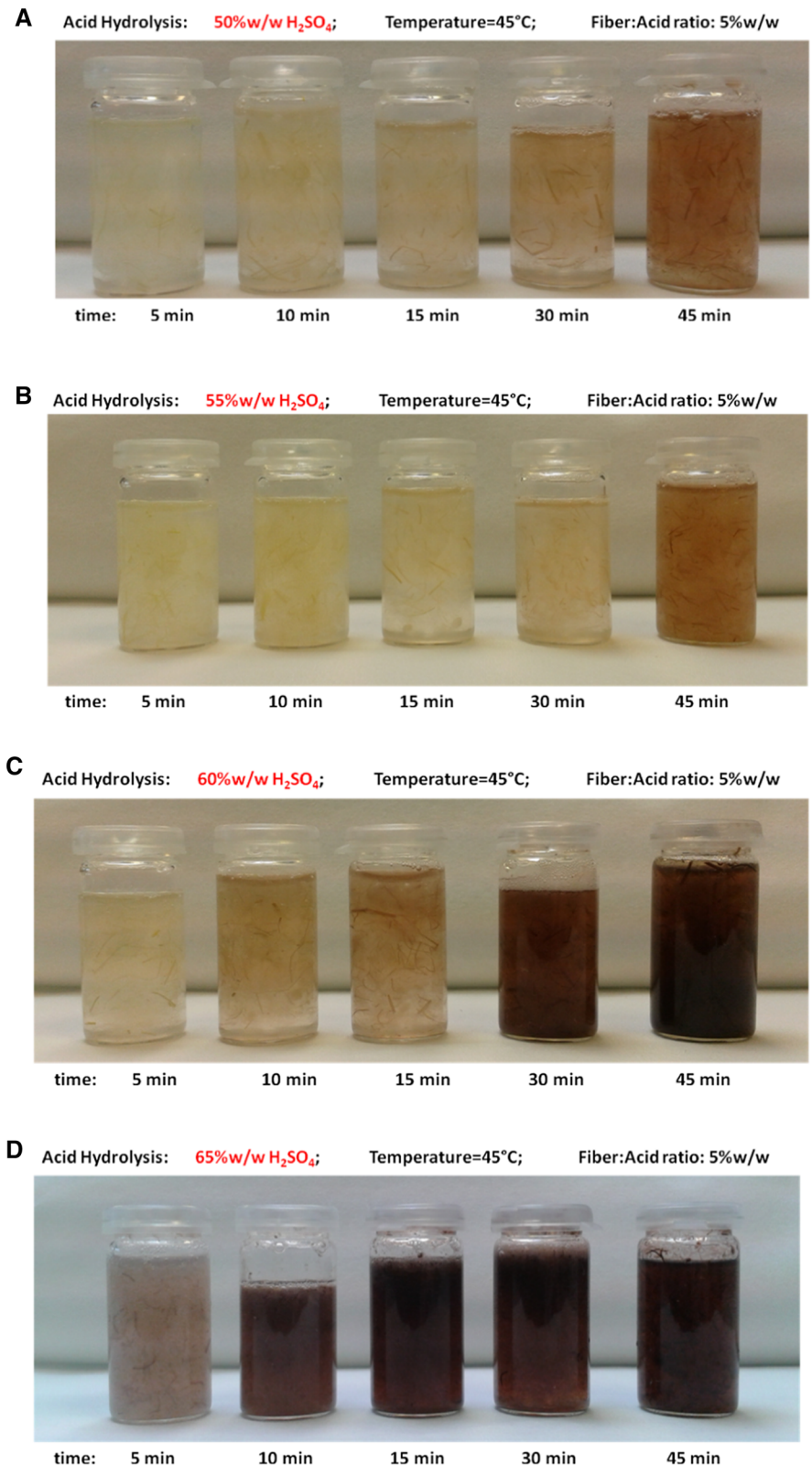

Fig. 2 Dispersions of phormium (*Phormium tenax*) fibers obtained after different durations of acid hydrolysis carried out at 45 °C with different concentrations of H_2SO_4: **a** 50, **b** 55, **c** 60, and **d** 65% w/w

Although the fiber length seemed to shorten with the duration of the reaction, none of the tested conditions allowed obtaining the typical clear, opaque and viscous CNC dispersions (Bondeson et al. 2006; Kassab et al. 2019). Furthermore, all the studied reaction conditions caused a blackening of the dispersion, which was accelerated by increasing the acid concentration. This behavior may have been favored due to residual lignin and/or hemicelluloses present in bleached fibers. Indeed, Dong et al. (1998) reported that lignin could undergo secondary reactions of dehydration and oxidation during hydrolysis conditions that conduct to dark dispersions. Du et al. (2016b) attributed it to the degradation of hemicelluloses.

However, other authors obtained CNC from different fiber sources using alkaline and peroxyde bleaching but with different hydrolysis conditions (Sfiligoj Smole et al. 2019; Ventura-Cruz and Tecante 2019). Nevertheless, Agarwal et al. (2018) obtained high-lignin-containing CNCs by using 64 wt% H_2SO_4 hydrolysis from poplar wood.

In contrast to our results, Fortunati et al. (2013) managed to obtain CNCs from phormium fibers with similar hydrolysis conditions (64% H_2SO_4 w/w at 45 °C for 30 min) but with a different pre-treatment of the fibers. First, they extracted the waxes with organic solvents, then bleached the fibers with $NaClO_2$ (0.7% w/v, 2 h boiling, pH = 4) and finally they carried out treatments with $NaHSO_3$ (5% w/v) and NaOH (17.5% w/v). These authors described that these pre-treatments were effective in removing lignin and hemicelluloses. After acid hydrolysis, they managed to obtain CNCs with acicular structure (d = 15 nm and L ≈ 150 nm) with a yield of 35%. The differences in the pre-treatments of the fibers, punctually in the bleaching reagents used as well as the order of the stages, could justify their success in obtaining CNCs.

Cellulose nanofibrils (CNFs)

Bleached phormium fibers were subjected to a refining process prior to the grinding treatment to obtain CNFs (Siró and Plackett 2010). During this refining process, the partial elimination of the primary wall of the fibers was favored by the shear stress produced in the PFI mill, leading to an increase in the flexibility of the fibers due to the breakage of its structure in thin layers (delamination or fibrillation). Then, the release of the fibrils occurred, thus increasing the specific surface area of the refined fibers. But if the refining process would prolong too much, the fibers might undergo shortening, which in some cases might be undesirable as fibers would show lower resistance and drainability (Nakagaito and Yano 2004). At the end of this process, bleached and refined phormium fibers (Fig. 1d), presented a drainability value of 74 ± 2°SR, which was very close to the optimum value (≈ 70°SR) required for the subsequent mechanical fibrillation (Desmaisons et al. 2017).

Bleached and refined phormium fibers were processed in the ultra-fine friction mill in order to obtain CNFs. During this process, the structure of the cell wall was broken by the shear forces generated by the equipment and the nano-sized fibers were individualized (Siró and Plackett 2010). CNFs were obtained after re-circulating the aqueous suspensions of bleached and refined phormium fibers 130 times. The number of cycles used was defined taking into account that after each step through the grinder the particles generally became smaller and more uniform in diameter, and that the mechanical treatment damaged the crystalline domains of cellulose and the energy required for the process increased (Vazquez et al. 2015).

Figure 3 shows the visual appearance of the aqueous CNF suspensions.

These suspensions exhibit a faint yellow coloration and a weak gel appearance that remained stable during storage in the refrigerator for at least 2 years. The solid content was 1.35% and its production process had a yield of 77% due to the fact that part of the solid was retained between the rotor and the stator of the grinder. The obtained yield is typical of this type of process. Ilyas et al. (2019) reported yields between 70 and 92% when producing CNFs from sugar palm fibers previously refined with a PFI mill. These authors noted that as the number of grinding cycles increased from 5 to 15, the performance of the process also increased and mechanical defibrillation of the fibers became more effective.

The nanofiber's morphology, observed by atomic force microscopy (AFM), is shown in Fig. 3, and its diameter and length calculated from these micrographs are shown in Table 3. CNFs occur as characteristics entangled and flexible filaments (Thomas et al. 2018), with an average diameter of 9.7 nm. It seems to be somewhat aggregated and, as they were

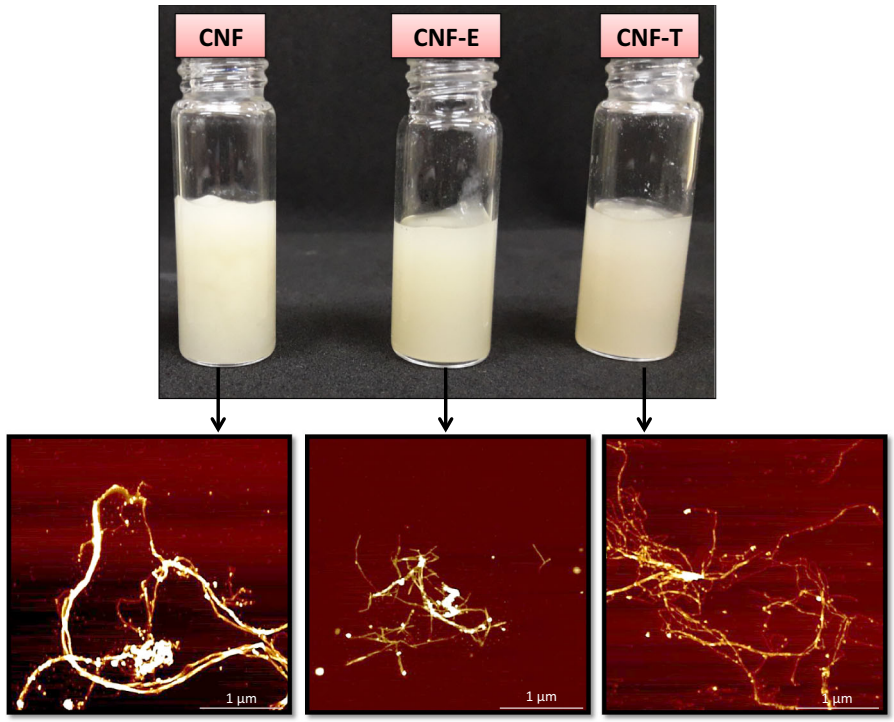

Fig. 3 Visual appearance and atomic force microscopy images of cellulose nanofibril dispersions prepared with bleached and refined phormium fibers (CNF), and with bleached and refined phormium fibers modified by endoglucanases and TEMPO-mediated oxidation treatments (CNF-E and CNF-T respectively)

Table 3 Solid content (%), diameter (nm), length (nm), crystallinity index (%) and Z potential (mV) for CNF, CNF-E and CNF-T

	CNF	CNF-E	CNF-T
Solid content (%)	1.35 ± 0.16^{b}	1.70 ± 0.12^{c}	0.82 ± 0.07^{a}
Diameter (nm)	9.67 ± 3.09^{b}	$6.84 \pm 3.13^{a,b}$	3.89 ± 1.97^{a}
Length (nm)	754–5741	406.74 ± 132.50	ND
Crystallinity index (%)	75.15 ± 4.64^{a}	83.60 ± 1.12^{b}	78.44 ± 0.59^{a}
Z potential (mV)	-0.7 ± 0.3^{a}	-0.1 ± 0.1^{a}	-50.7 ± 2.4^{b}

ND not determined

Values with different letters in the same row are significantly different ($p < 0.05$) according to the Tukey's test

rolled up, it was only possible to determine its length in some cases, varying from ≈ 750 to 5750 nm (Table 3). These nanofibers were significantly thinner than those reported by Ortiz et al. (2018), who obtained CNFs with d = 50–60 nm and L = 485 ± 2 µm from bleached but not refined phormium fibers. The refining process seems to avoid nanofiber aggregation and favor its disintegration.

The source of cellulose also seems to influence the size of the resulting nanofibers. In this sense, Claro et al. (2018) reported that CNFs prepared from eucalyptus leaves had a diameter of 17 nm and a length of 1100 nm while those prepared from *Curaua* leaves had diameter greater than 36 nm and length that could not be determined; while Hassan et al. (2012) obtained CNFs from bagasse and rice straw with diameter of 5–15 and 4–13 nm, respectively.

The X-ray diffractogram for CNFs prepared from bleached and refined phormium fibers are shown in Fig. 4a. A clearly defined peak is observed at $2\theta = 22.9°$ corresponding to the crystallographic plane 200 (Bras et al. 2010; Ling et al. 2019) together with less marked and broader peaks at $2\theta = 14°–16°$ corresponding to planes 1–10 and 110, and a slight rise around $2\theta = 35°$ that is attributed to the 004 plane. All these signals are characteristic of Iβ type cellulose.

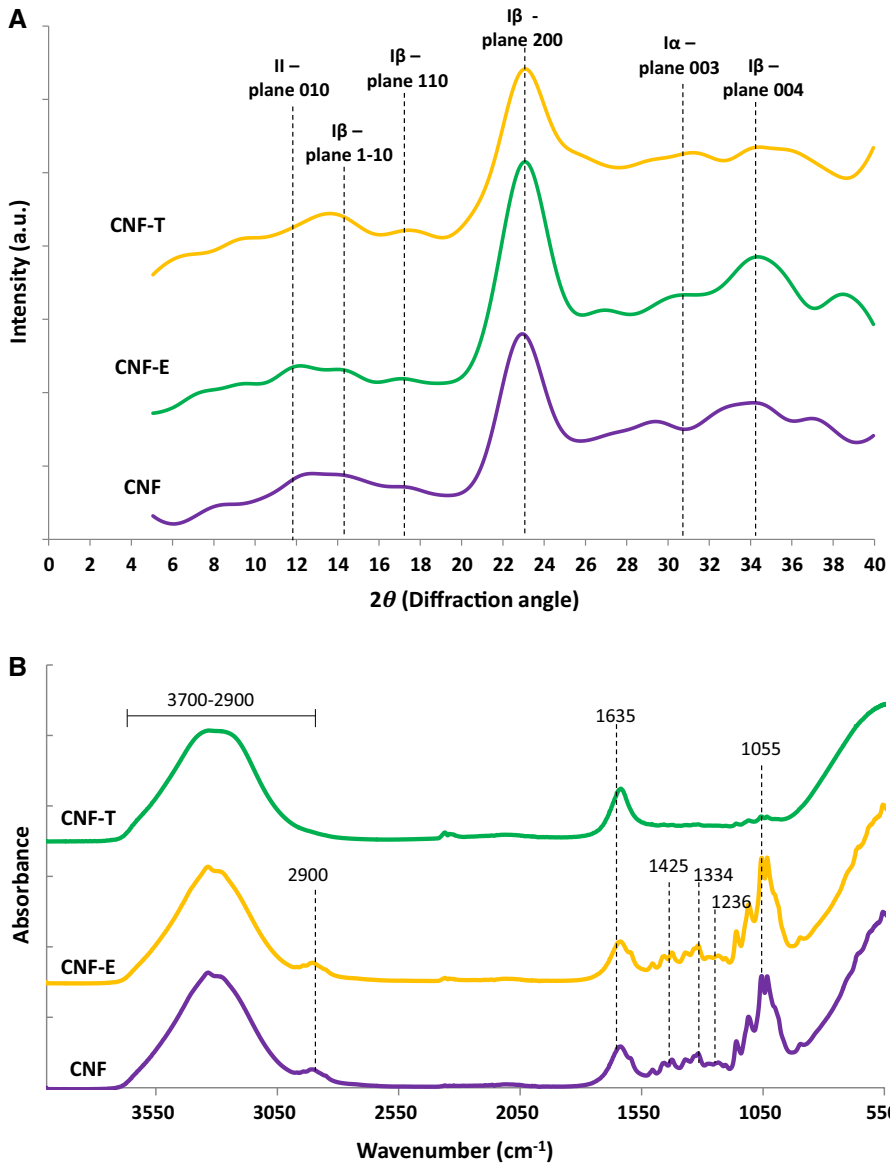

Fig. 4 X-ray diffractograms (**a**) and ATR-FTIR spectra (**b**) for CNF, CNF-E and CNF-T

Two additional peaks are also observed at ≈ 12° and ≈ 31° in the X-ray diffraction patterns, and could be attributed to plane 010 of cellulose II and to plane 003 of cellulose Iα, respectively (French 2014; Ling et al. 2019), as well as other peaks that were not expected for any of the known cellulose allomorphs. Similar patterns were reported for initial phormium fibers by Fortunati et al. (2013) and Efendy and Pickering (2014), who reported a crystallinity index of 68.5% for this raw material. The crystallinity index calculated for CNF (Table 3) was ≅ 72%, slightly higher than the value reported for original fibers due to shear and impact forces experienced during grinding that can induce partial degradation and removal of amorphous cellulose (Borsoi et al. 2016). However, it is worth noting that the crystallinity index obtained from the Segal equation is only indicative because of the presence of compounds other than cellulose I. This value is significantly higher than the one reported by Ortiz et al. (2018) for CNF prepared from bleached but not refined phormium fibers (CrI = 35.5%) and those reported by other authors (54–64%) for CNF extracted from flax, eucalyptus and wood (Lavoine et al. 2012).

However, it is similar to the one reported by Borsoi et al. (2016) and Leite et al. (2017).

Table 3 also shows the Z-potential value for CNFs under study. CNFs have a Z-potential value close to zero, significantly lower in absolute value than the one reported by other authors (− 13 to − 19 mV) for CNF obtained from carrot and eucalyptus fibers (Guimarães et al. 2016). Although the absence of surface charge would be indicative of instability or propention to sedimentation (Cano-Sarmiento et al. 2018), the aqueous suspension of CNF did not show any visible sign of destabilization during refrigerated storage for at least 2 years. This may be due to the concentration of the CNF suspensions, as sedimentation was observed by other authors working with lower concentrations. This stability may be due to the rheology of the suspensions. For dilute CNF suspensions (like 0.1 wt%), the fibers cannot form an interconnected network that influences the rheology, whereas a gel-like behavior is observed for higher concentrations (Mendoza et al. 2018). Entanglement of the nanofibers promotes the colloidal stability of the suspension.

The ATR-FTIR spectrum for CNF, shown in Fig. 4b, exhibits a wide band at 3700–2900 cm^{-1} (with a broad peak at 3330 cm^{-1}) associated with O–H groups stretching in inter- and intramolecular hydrogen bonds, a peak at 2900 cm^{-1} attributed to the C–H bond stretching and another one at 1635 cm^{-1} corresponding to the O–H bond flexion of absorbed water. It also showed the typical cellulose bands, attributed to "scissors" (1425 cm^{-1}) and "swinging" type movements of the $–CH_2$ group (1334 and 1318 cm^{-1}), to C–H bond flexion and stretching (1370 and 1206 cm^{-1}, respectively) and to the C–O bond stretching (at 1110, 1055, 1033, and 987 cm^{-1}). However, other peaks are observed corresponding to lignin, associated to the CH bond vibration, to C=O stretching and to the CH bond deformation of the $–CH_2$ and $–CH_3$ groups (at 1593, 1506, and 1459 cm^{-1}), and to the presence of p-hydroxyphenyl units (at 833 cm^{-1}). In addition, peaks at 1236 and 2900 cm^{-1} can also be associated with the vibrations of the bonds that make up the skeleton of hemicellulose (Ko et al. 2015). These results confirm the presence of lignin and hemicelluloses in CNF proving that the bleaching treatment with H_2O_2 was not effective to completely eliminate them from phormium fibers, in agreement with Ortiz et al. (2018). Nevertheless, although their presence did not seem to affect the preparation of CNF it did so during the synthesis of CNC, as mentioned before.

Cellulose nanofibrils obtained after endoglucanase and TEMPO-mediated oxidation treatments (CNF-E and CNF-T)

In this work, bleached and refined phormium fibers were subjected to an enzymatic treatment with endoglucanases or to a TEMPO-mediated oxidation treatment before being processed in the ultra-fine friction grinder in order to optimize the production process of CNFs and modify the fiber characteristics (Kargarzadeh et al. 2018). Thus CNF-E and CNF-T were obtained, respectively, at the end of these processes.

It is known that cellulose needs a set of enzymes, the cellulases, to be completely degraded in nature (Trache et al. 2017). The specific effect on cellulose fibers depends on the cellulase type, in addition to the reaction conditions and the substrate used (Missoum et al. 2013). In particular endoglucanases can hydrolyze the amorphous regions of cellulose. The CNF-E suspension shown in Fig. 3 presents a solid content of 1.7% (Table 3). The yield of its process was significantly lower ($\approx$ 66.5%) than the one for obtaining CNF, possibly due to the solid loss by solubilization during washing performed after stopping the enzymatic reaction. CNF-E also present a rod shape (Fig. 3) and smaller dimensions than for CNF. In this case, the nanofibers present an average diameter and length of 6.8 and 406 nm, respectively (Table 3), as determined by AFM images analysis. Other authors reported similar dimensions for cellulose nanofibrils from sisal fibers (Siqueira et al. 2010) and wood fibers (Henriksson et al. 2007) previously treated with endoglucanases. It is evident that enzymatic hydrolysis decreases the length of the fibers, but also facilitates their disintegration/delamination by destabilization of the hydrogen bonding between the microfibrils and prevents the homogenizer blocking (Missoum et al. 2013). These enzymes seem to be more efficient to degrade amorphous cellulose domains, increasing significantly the crystallinity of CNF-E with respect to CNF (Table 3). Similar results were found by Zhu et al. (2011), Saelee et al. (2016) and Long et al. (2017). Long et al. (2017) also reported a similar CrI for nanofibers extracted from pine wood regardless the type of enzyme used for the pre-

treatment (xylanases and endoglucases). Andersen (2007) reported that it is necessary to eliminate lignin from the fibers before the enzymatic hydrolysis since the cellulases could interact irreversibly with this compound. So, depending on the location of the remaining lignin in the phormium fibers, the activity of the enzyme could be somewhat impeded or lower than expected. On the other hand, and as expected, CNF-E presented a Z-potential value (Table 3) and ATR-FTIR spectrum (Fig. 4b) similar to those observed for CNF, showing that the enzymatic treatment did not change the surface charge of these nanofibers or their chemical nature.

Regarding the chemical treatment used in this work, the 2,2,6,6-tetramethylpiperidine-1-oxyl radical (TEMPO) was used to oxidize bleached and refined phormium fibers, before being mechanically grinded. In this way an aqueous suspension of nanofibers was obtained, named CNF-T. Through this treatment, the selective oxidation of the hydroxyl groups of the primary alcohols (–OH of C6) to aldehydes (carbonyl groups –COH) or to carboxylic acids (carboxyl-COOH groups) takes place, thus modifying the surface of the microfibrils (Dufresne 2017). The aqueous suspension of CNF-T had a solid content of 0.82% (Table 3); significantly lower than of the one for CNF and CNF-E. It should be noted that in this case the aqueous dispersion of bleached and refined phormium fibers had a concentration of 1% w/v, while in the other processes the initial concentration of fibers used was doubled. The yield of the process was 73%, being slightly lower than the one described for obtaining CNF, possibly due to the loss of solid by solubilization during washing carried out after the chemical treatment. Gamelas et al. (2015) reported similar yields in obtaining nanofibers from eucalyptus fibers bleached and treated with TEMPO; whereas Besbes et al. (2011) achieved superior performance (88%) by processing bleached and oxidized pine fibers with TEMPO.

CNF-T was the only cellulose nanofibrils studied that presented surface charge, with a Z-potential = − 50.7 mV (Table 3) due to the ionized carboxylate groups introduced to the surface when oxidizing cellulose. Similar results were reported by Benhamou et al. (2014) and Gamelas et al. (2015) for nanofibers produced from palm (− 59 mV) and eucalyptus (− 46 mV) fibers, respectively. The morphology of CNF-T is shown in Fig. 3. It was possible to determine by AFM the diameter of the nanofibers but not their length because they consist of very long fragments. The diameter for CNF-T (3.9 nm) was found to be significantly lower than the one reported for CNF and CNF-E (Table 3). In this case, it was observed that the nanofibers were completely individualized, without finding the presence of aggregates. These observations agree with Siqueira et al. (2010) that observed that this chemical treatment facilitates the separation of the nanofibers and prevents their subsequent aggregation due to the repulsive forces of the surface carboxylate groups. Jiang and Hsieh (2013) also found that nanofibers obtained from rice straw pre-treated with TEMPO had smaller diameter than those that had been subjected directly to mechanical treatment ($\approx$ 1.7 nm vs $\approx$ 12 nm) and pointed out that the smaller diameter gave them greater flexibility and specific surface.

On the other hand, CNF-T showed a CrI $\approx$ 78% (Table 3) that did not show significant difference with of the one observed for CNF. The same behavior was reported by Besbes et al. (2011) and Benhamou et al. (2014) for eucalyptus and palm nanofibers, respectively, that was attributed to the fact that the chemical reaction would not take place in the crystalline zones of cellulose I.

TEMPO treatment modified the chemical structure of the nanofibers and this could be observed in the ATR-FTIR spectrum shown in Fig. 4b. A wide band at 3700–2800 cm^{-1} associated with the stretching of the OH bonds of inter- and intramolecular hydrogen bonds and other at 2900–2800 cm^{-1} attributed to the stretching of the CH bond can be identified. The peak at 1635 cm^{-1} could be attributed to the flexion of the OH bond of the absolved water, but can be overlapped with the one of carboxyl groups at approximately 1630 cm^{-1}, product of the action of TEMPO on cellulose. Hay (2007) explains that the protonated carboxylic acid produces absorption bands corresponding to the stretching of the carbonyl group (C=O) between 1690 and 1750 cm^{-1}, and vibrations of C–OH between 1200 and 1300 cm^{-1}. In the deprotonation, the vibrational stretching of the C=O changes to a lower energy as its vibratory mode is coupled to the one of the other oxygen, giving rise to an asymmetric characteristic vibration between 1540 and 1650 cm^{-1}. Similarly, the C–OH band changes to a higher energy in deprotonation, producing a symmetric COO mode between 1300 and 1420 cm^{-1}. In both cases they were more prominent than in CNF and

CNF-E spectra. All peaks previously described in the 1600–900 cm^{-1} zone are present in CNF-T spectrum but with lower intensities, while the one at 833 cm^{-1} attributed to p-hydroxyphenyl units was not observed, suggesting that lignin could have also been oxidized during the test. Similar results were obtained by Benhamou et al. (2014) who also observed the peak near 1730 cm^{-1} and attributed it to the CO stretching of carboxyl group in its acid form for CNF coming from the spine and leaves of *Phoenix dactylifera* L. (palm tree) pre-oxidized by TEMPO. Cao et al. (2012) reported the appearance of two absorption bands at 1601 and 1410 cm^{-1} in the FTIR spectrum for jute CNF derived from TEMPO-mediated oxidation of hydroxyl groups at the C6 position to sodium carboxylate.

Conclusions

Cellulose nanofibrils with different characteristics in terms of size, crystallinity and surface charge have been obtained from phormium fibers by a mechanical disintegration process with and without endoglucanases or TEMPO-mediated oxidation pretreatments. However, cellulose nanocrystals were not obtained by acid hydrolysis from the same alkali treated and bleached fibers under known and effective conditions. It seems that the presence of residual lignin and hemicelluloses could interfere with the hydrolysis reaction, giving the fibers a charred appearance. This behavior evidences that the initial state of phormium fibers and the presence of other components such as lignin and hemicelluloses, affect the process efficiency of CNCs but not that of CNFs.

Acknowledgments The authors are thankful to the Universidad Nacional de La Plata (11/X618 and 11/X750), Consejo Nacional de Investigaciones Científicas y Técnicas (CONICET+CNRS) and Agencia Nacional de Promoción Científica y Tecnológica (PICT-2013-2124 and PICT-2015-2822) for their financial support. LGP2 is part of the LabEx Tec 21 (Investissements d'Avenir - Grant Agreement n°ANR-11-LABX-0030) and of the PolyNat Carnot Institut (Investissements d'Avenir - Grant Agreement n°ANR-11-CARN-030-01).

References

Abdul Khalil HPS, Davoudpour Y, Islam MN et al (2014) Production and modification of nanofibrillated cellulose using various mechanical processes: a review. Carbohydr Polym 99:649–665. https://doi.org/10.1016/j.carbpol.2013.08.069

Agarwal UP, Ralph SA, Reiner RS et al (2018) Production of high lignin-containing and lignin-free cellulose nanocrystals from wood. Cellulose 25:5791–5805. https://doi.org/10.1007/s10570-018-1984-z

Andersen N (2007) Enzymatic hydrolysis of cellulose: experimental and modelling studies. In: PhD thesis, BioCentrum., Technical University of Denmark, Lyngby, Denmark

Beltramino F, Roncero MB, Vidal T, Valls C (2018) A novel enzymatic approach to nanocrystalline cellulose preparation. Carbohydr Polym 189:39–47

Benhamou K, Dufresne A, Magnin A et al (2014) Control of size and viscoelastic properties of nanofibrillated cellulose from palm tree by varying the TEMPO-mediated oxidation time. Carbohydr Polym 99:74–83. https://doi.org/10.1016/j.carbpol.2013.08.032

Besbes I, Alila S, Boufi S (2011) Nanofibrillated cellulose from TEMPO-oxidized eucalyptus fibres: effect of the carboxyl content. Carbohydr Polym 84:975–983. https://doi.org/10.1016/j.carbpol.2010.12.052

Bondeson D, Mathew A, Oksman K (2006) Optimization of the isolation of nanocrystals from microcrystalline cellulose by acid hydrolysis. Cellulose 13:171–180. https://doi.org/10.1007/s10570-006-9061-4

Börjesson M, Westman G (2015) Crystalline nanocellulose—preparation, modification, and properties. In: Cellulose-fundamental aspects and current trends. IntechOpen

Borsoi C, Zimmernnam MVG, Zattera AJ et al (2016) Thermal degradation behavior of cellulose nanofibers and nanowhiskers. J Therm Anal Calorim 126:1867–1878. https://doi.org/10.1007/s10973-016-5653-x

Bras J, Hassan ML, Bruzesse C et al (2010) Mechanical, barrier, and biodegradability properties of bagasse cellulose whiskers reinforced natural rubber nanocomposites. Ind Crops Prod 32:627–633

Cano-Sarmiento C, Téllez-Medina DI, Viveros-Contreras R et al (2018) Zeta potential of food matrices. Food Eng Rev 10:113–138. https://doi.org/10.1007/s12393-018-9176-z

Cao X, Ding B, Yu J, Al-Deyab SS (2012) Cellulose nanowhiskers extracted from TEMPO-oxidized jute fibers. Carbohydr Polym 90:1075–1080. https://doi.org/10.1016/j.carbpol.2012.06.046

Claro PIC, Corrêa AC, de Campos A et al (2018) Curaua and eucalyptus nanofibers films by continuous casting: mechanical and thermal properties. Carbohydr Polym 181:1093–1101. https://doi.org/10.1016/j.carbpol.2017.11.037

De Rosa IM, Kenny JM, Puglia D et al (2010) Tensile behavior of New Zealand flax (Phormium tenax) fibers. J Reinf Plast Compos 29:3450–3454

Desmaisons J, Boutonnet E, Rueff M et al (2017) A new quality index for benchmarking of different cellulose nanofibrils. Carbohydr Polym 174:318–329. https://doi.org/10.1016/j.carbpol.2017.06.032

Dong XM, Revol J-F, Gray DG (1998) Effect of microcrystallite preparation conditions on the formation of colloid crystals of cellulose. Cellulose 5:19–32

Du H, Liu C, Mu X et al (2016a) Preparation and characterization of thermally stable cellulose nanocrystals via a sustainable approach of FeCl3-catalyzed formic acid hydrolysis. Cellulose 23:2389–2407. https://doi.org/10.1007/s10570-016-0963-5

Du H, Liu C, Zhang Y et al (2016b) Preparation and characterization of functional cellulose nanofibrils via formic acid hydrolysis pretreatment and the followed high-pressure homogenization. Ind Crops Prod 94:736–745

Dufresne A (2017) Nanocellulose: from nature to high performance tailored materials. Walter de Gruyter GmbH & Co KG, Berlin

Efendy MGA, Pickering KL (2014) Comparison of harakeke with hemp fibre as a potential reinforcement in composites. Compos A Appl Sci Manuf 67:259–267. https://doi.org/10.1016/j.compositesa.2014.08.023

Fortunati E, Luzi F, Puglia D et al (2014) Investigation of thermo-mechanical, chemical and degradative properties of PLA-limonene films reinforced with cellulose nanocrystals extracted from Phormium tenax leaves. Eur Polym J 56:77–91. https://doi.org/10.1016/j.eurpolymj.2014.03.030

Fortunati E, Puglia D, Monti M et al (2013) Extraction of cellulose nanocrystals from Phormium tenax fibres. J Polym Environ 21:319–328. https://doi.org/10.1007/s10924-012-0543-1

Foster EJ, Moon RJ, Agarwal UP et al (2018) Current characterization methods for cellulose nanomaterials. Chem Soc Rev 47:2609–2679. https://doi.org/10.1039/C6CS00895J

French AD (2014) Idealized powder diffraction patterns for cellulose polymorphs. Cellulose 21:885–896

Gamelas JAF, Pedrosa J, Lourenço AF et al (2015) On the morphology of cellulose nanofibrils obtained by TEMPO-mediated oxidation and mechanical treatment. Micron 72:28–33. https://doi.org/10.1016/j.micron.2015.02.003

Gómez HC, Serpa A, Velásquez-Cock J et al (2016) Vegetable nanocellulose in food science: a review. Food Hydrocoll 57:178–186. https://doi.org/10.1016/j.foodhyd.2016.01.023

Guimarães IC, dos Reis KC, Menezes EGT et al (2016) Cellulose microfibrillated suspension of carrots obtained by mechanical defibrillation and their application in edible starch films. Ind Crops Prod 89:285–294. https://doi.org/10.1016/j.indcrop.2016.05.024

Hassan ML, Mathew AP, Hassan EA et al (2012) Nanofibers from bagasse and rice straw: process optimization and properties. Wood Sci Technol 46:193–205. https://doi.org/10.1007/s00226-010-0373-z

Hay MB (2007) Advances in the molecular-scale understanding of geochemical processes: carboxyl structures in natural organic matter, organosulfur cycling in soils, and the coordination chemistry of aqueous aluminum. Princeton University, Princeton

Henriksson M, Henriksson G, Berglund LA, Lindström T (2007) An environmentally friendly method for enzyme-assisted preparation of microfibrillated cellulose (MFC) nanofibers. Eur Polym J 43:3434–3441. https://doi.org/10.1016/j.eurpolymj.2007.05.038

Ilyas RA, Sapuan SM, Ishak MR, Zainudin ES (2019) Sugar palm nanofibrillated cellulose (Arenga pinnata (Wurmb.) Merr): effect of cycles on their yield, physic-chemical, morphological and thermal behavior. Int J Biol Macromol 123:379–388. https://doi.org/10.1016/j.ijbiomac.2018.11.124

Jawaid M, Boufi S, Abdul Khalil HPS (2017) Cellulose-reinforced nanofibre composites: production, properties and applications. Woodhead Publishing, Sawston

Jiang F, Hsieh Y-L (2013) Chemically and mechanically isolated nanocellulose and their self-assembled structures. Carbohydr Polym 95:32–40. https://doi.org/10.1016/j.carbpol.2013.02.022

Kargarzadeh H, Mariano M, Gopakumar D et al (2018) Advances in cellulose nanomaterials. Cellulose 25:2151–2189. https://doi.org/10.1007/s10570-018-1723-5

Kasiri N, Fathi M (2018) Production of cellulose nanocrystals from pistachio shells and their application for stabilizing Pickering emulsions. Int J Biol Macromol 106:1023–1031. https://doi.org/10.1016/j.ijbiomac.2017.08.112

Kassab Z, Aziz F, Hannache H et al (2019) Improved mechanical properties of k-carrageenan-based nanocomposite films reinforced with cellulose nanocrystals. Int J Biol Macromol 123:1248–1256. https://doi.org/10.1016/j.ijbiomac.2018.12.030

Ko JK, Kim Y, Ximenes E, Ladisch MR (2015) Effect of liquid hot water pretreatment severity on properties of hardwood lignin and enzymatic hydrolysis of cellulose. Biotechnol Bioeng 112:252–262. https://doi.org/10.1002/bit.25349

Lavoine N, Desloges I, Dufresne A, Bras J (2012) Microfibrillated cellulose—its barrier properties and applications in cellulosic materials: a review. Carbohydr Polym 90:735–764

Leite ALMP, Zanon CD, Menegalli FC (2017) Isolation and characterization of cellulose nanofibers from cassava root bagasse and peelings. Carbohydr Polym 157:962–970. https://doi.org/10.1016/j.carbpol.2016.10.048

Li Q, Wang A, Long K et al (2018) Modified Fenton oxidation of cellulose fibers for cellulose nanofibrils preparation. ACS Sustain Chem Eng 7:1129–1136

Ling Z, Wang T, Makarem M et al (2019) Effects of ball milling on the structure of cotton cellulose. Cellulose 26:305–328

Long L, Tian D, Hu J et al (2017) A xylanase-aided enzymatic pretreatment facilitates cellulose nanofibrillation. Bioresour Technol 243:898–904. https://doi.org/10.1016/j.biortech.2017.07.037

Mendoza L, Batchelor W, Tabor RF, Garnier G (2018) Gelation mechanism of cellulose nanofibre gels: a colloids and interfacial perspective. J Colloid Interface Sci 509:39–46. https://doi.org/10.1016/j.jcis.2017.08.101

Mishra S, Kharkar PS, Pethe AM (2018) Biomass and waste materials as potential sources of nanocrystalline cellulose: comparative review of preparation methods (2016-Till date). Carbohydr Polym 207:418–427

Missoum K, Belgacem M, Bras J (2013) Nanofibrillated cellulose surface modification: a review. Materials (Basel) 6:1745–1766

Nakagaito AN, Yano H (2004) The effect of morphological changes from pulp fiber towards nano-scale fibrillated

cellulose on the mechanical properties of high-strength plant fiber based composites. Appl Phys A 78:547–552

Nasir M, Hashim R, Sulaiman O, Asim M (2017) 11: Nanocellulose: preparation methods and applications. In: Jawaid M, Boufi S, Abdul Khalil HPS (eds) Cellulose-reinforced nanofibre composites. Woodhead Publishing, Sawston, pp 261–276

Niu X, Liu Y, Song Y et al (2018) Rosin modified cellulose nanofiber as a reinforcing and co-antimicrobial agents in polylactic acid /chitosan composite film for food packaging. Carbohydr Polym 183:102–109. https://doi.org/10.1016/j.carbpol.2017.11.079

Ortiz CM, Salgado PR, Dufresne A, Mauri AN (2018) Microfibrillated cellulose addition improved the physicochemical and bioactive properties of biodegradable films based on soy protein and clove essential oil. Food Hydrocoll 79:416–427. https://doi.org/10.1016/j.foodhyd.2018.01.011

Panaitescu DM, Frone AN, Nicolae C (2013) Micro-and nanomechanical characterization of polyamide 11 and its composites containing cellulose nanofibers. Eur Polym J 49:3857–3866

Rohaizu R, Wanrosli WD (2017) Sono-assisted TEMPO oxidation of oil palm lignocellulosic biomass for isolation of nanocrystalline cellulose. Ultrason Sonochem 34:631–639

Saelee K, Yingkamhaeng N, Nimchua T, Sukyai P (2016) An environmentally friendly xylanase-assisted pretreatment for cellulose nanofibrils isolation from sugarcane bagasse by high-pressure homogenization. Ind Crops Prod 82:149–160. https://doi.org/10.1016/j.indcrop.2015.11.064

Sfiligoj Smole M, Hribernik S, Kurečič M, Krajnc AU, Kreže T, Kleinschek KS (2019) Surface properties of non-conventional cellulose fibres. In: Biobased polymers, 1 edn. Springer International Publishing, pp XVII-88. https://doi.org/10.1007/978-3-030-10407-8

Siqueira G, Bras J, Dufresne A (2010) Cellulosic bionanocomposites: a review of preparation, properties and applications. Polymers (Basel) 2:728

Siró I, Plackett D (2010) Microfibrillated cellulose and new nanocomposite materials: a review. Cellulose 17:459–494

Sirviö JA, Visanko M (2017) Anionic wood nanofibers produced from unbleached mechanical pulp by highly efficient chemical modification. J Mater Chem A 5:21828–21835

Thomas B, Raj MC et al (2018) Nanocellulose, a versatile green platform: from biosources to materials and their applications. Chem Rev 118:11575–11625. https://doi.org/10.1021/acs.chemrev.7b00627

Tibolla H, Pelissari FM, Menegalli FC (2014) Cellulose nanofibers produced from banana peel by chemical and enzymatic treatment. LWT Food Sci Technol 59:1311–1318. https://doi.org/10.1016/j.lwt.2014.04.011

Trache D, Hussin MH, Haafiz MKM, Thakur VK (2017) Recent progress in cellulose nanocrystals: sources and production. Nanoscale 9:1763–1786. https://doi.org/10.1039/C6NR09494E

Vazquez A, Foresti ML, Moran JI, Cyras VP (2015) Extraction and production of cellulose nanofibers. In: Pandey JK, Takagi H, Nakagaito AN, Kim H-J (eds) Handbook of polymer nanocomposites. Processing, performance and application. Springer, Berlin, pp 81–118

Ventura-Cruz S, Tecante A (2019) Extraction and characterization of cellulose nanofibers from Rose stems (Rosa spp.). Carbohydr Polym 220:53–59. https://doi.org/10.1016/j.carbpol.2019.05.053

Xie H, Du H, Yang X, Si C (2018) Recent strategies in preparation of cellulose nanocrystals and cellulose nanofibrils derived from raw cellulose materials. Int J Polym Sci. https://doi.org/10.1155/2018/7923068

Zainuddin SYZ, Ahmad I, Kargarzadeh H et al (2013) Potential of using multiscale kenaf fibers as reinforcing filler in cassava starch-kenaf biocomposites. Carbohydr Polym 92:2299–2305

Zhou Y, Saito T, Bergström L, Isogai A (2018) Acid-free preparation of cellulose nanocrystals by TEMPO oxidation and subsequent cavitation. Biomacromol 19:633–639

Zhu JY, Sabo R, Luo X (2011) Integrated production of nanofibrillated cellulose and cellulosic biofuel (ethanol) by enzymatic fractionation of wood fibers. Green Chem 13:1339–1344. https://doi.org/10.1039/C1GC15103G